ELSEVIER Applied Mathematics and Computation 124 (2001) 215–226
APPLIED MATHEMATICS AND COMPUTATION
www.elsevier.com/locate/amc

Optimization of convergence acceleration in multigrid numerical solutions of conductive–convective problems

J.A. Rabi, M.J.S. de Lemos *

Departamento de Energia – IEME, Instituto Tecnológico de Aeronáutica – ITA/CTA, 12.228-900 São José dos Campos, São Paulo, Brazil

Abstract

The present work investigates the existence of optimal algorithm parameters for multigrid numerical solutions of a two-dimensional steady-state conductive–convective problem. The velocity field inside the rectangular domain and the temperature distribution at its four boundaries are known and kept constant. The numerical method includes finite volume discretization and Weighted Upstream Differencing Scheme (WUDS) interpolation on structured, orthogonal and regular meshes. Multigrid is implemented according to the correction storage (CS) formulation. Minimum computational effort is sought as a function of control-volume Peclet number, different numbers of grids, number of smoothing sweeps in each level and distinct combinations of iterative solution algorithm.

Keywords: Multigrid; Numerical methods; Laminar flow; Viscous flow; Computational methods

1. Introduction

Multigrid methods are known for their ability to accelerate the convergence rate of iterative numerical solutions, which is desirable or even indispensable when well-refined meshes are employed. Accordingly, in single-grid methods these rates are greatest in the beginning of calculations, slowing down sen-

* Corresponding author.
E-mail address: mdelemos@tecsat.com.br (M.J.S. de Lemos).

0096-3003/01/$ - see front matter
PII: S0096-3003(00)00088-6

sibly as the iterative process goes on, increasing the necessary computational effort.

A Fourier spectral analysis relates the reason of such behavior to the iterative method capability of reducing efficiently only those error components whose wavelengths are smaller than or comparable to the grid spacing [3,4,18]. This is when multigrid methods play a major role by covering a broader wavelength spectrum through the iteration at a sequence of gradually less refined grids. Long wavelengths in a fine mesh become smaller in a coarse one, where they can then be better smoothed, accelerating convergence.

However, as Hackbusch [4] points out, no multigrid algorithm can be implemented as a 'black-box', with optimal parameters being usually found by inspection. Motivated by this, in this paper a steady-state conductive–convective problem is numerically solved by applying a multigrid method where parameters are varied and the corresponding overall performance are observed and compared. Among these changing strategies are physical conditions (Peclet numbers), number of grid levels, multigrid cycling, number of smoothing sweeps and choice of iterative solution algorithm. The numerical method also includes finite volume discretization over regular, orthogonal and structured grids, *Weighted Upstream Differencing Scheme* (WUDS) to perform interpolation and correction storage (CS) multigrid formulation.

2. Mathematical model

The physical problem investigated by this work involves a two-dimensional steady-state conduction–convection heat transfer with no internal heat sources. The velocity field inside the rectangular domain and the temperature distribution at all boundaries are known and fixed conditions, as sketched in Fig. 1.

Since assuming fixed values for the velocity components solves the hydrodynamic problem, it only remains to obtain the solution of the energy equation (in Cartesian coordinates), which for the present conditions reduces to [2]

$$\frac{\partial}{\partial x}(\rho UT) + \frac{\partial}{\partial y}(\rho VT) = \frac{\partial}{\partial x}\left(\frac{K}{C_p}\frac{\partial T}{\partial x}\right) + \frac{\partial}{\partial y}\left(\frac{K}{C_p}\frac{\partial T}{\partial y}\right), \tag{1}$$

where in the cases studied, all physical quantities are kept constant, except for the temperature T, which is the unknown to be numerically treated.

The values adopted for the fluid properties are $K/C_p = 1$ kg/m s and $\rho = 1$ kg/m^3 while the velocity components U and V assume 0 or 10 m/s (V actually assumes -10 m/s). The strictly conductive problem ($U = V = 0$) admits an analytical solution, which for the boundary conditions shown in Fig. 1 is given by

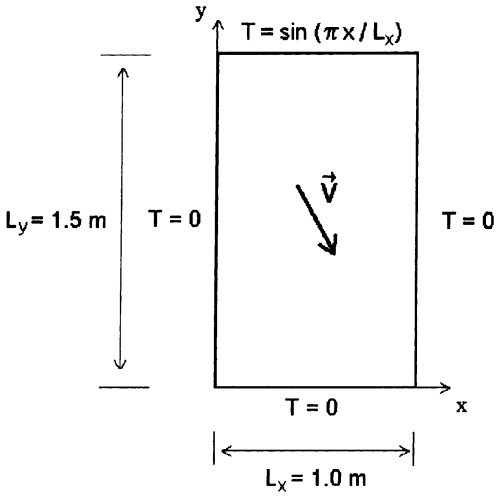

Fig. 1. Sketch of the conductive–convective problem and boundary conditions.

$$T(x,y) = \frac{\sinh(\pi y/L_x)}{\sinh(\pi L_y/L_x)} \sin\left(\frac{\pi x}{L_x}\right). \tag{2}$$

3. Numerical method

3.1. Finite volume discretization

Discretization is accomplished by building up structured, orthogonal and regular meshes according to a cell-centered scheme. Algebraic equations are obtained after integrating Eq. (1) over a typical control volume [9] sketched in Fig. 2.

Internodal interpolation follows the WUDS proposed by Raithby and Torrance [16]. It employs two coefficients α and β to weigh convective and diffusive processes at the control-volume interface. Taking the east face as an example, the temperature and its gradient (both presumed to be constant over the entire interface) are respectively approximated by

$$T_e = \left(\frac{1}{2} + \alpha_e\right) T_P + \left(\frac{1}{2} - \alpha_e\right) T_E \quad \text{and} \quad \left.\frac{\partial T}{\partial x}\right|_e = \beta_e \left(\frac{T_E - T_P}{\Delta x_e}\right). \tag{3}$$

The weighting coefficients are expressed as [15],

$$\alpha_e = \frac{Pe_e^2}{10 + 2Pe_e^2} \quad \text{and} \quad \beta_e = \frac{1 + 0.005Pe_e^2}{1 + 0.05Pe_e^2}, \tag{4}$$

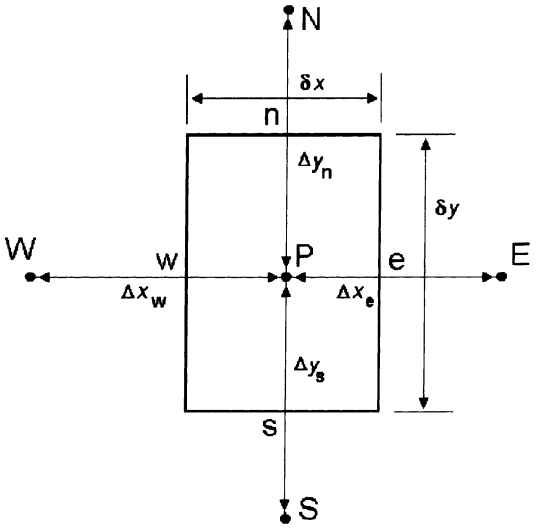

Fig. 2. Sketch and nomenclature of control volume to perform discretization.

where Pe_e is the control-volume Peclet number defined as

$$Pe_e = \left.\frac{\rho U \Delta x}{K/C_p}\right|_e. \tag{5}$$

The discretized energy equation is finally obtained after applying Eq. (3) to all four interfaces and inserting the resulting equations in Eq. (1) (integrated over the control volume):

$$a_P T_P = a_E T_E + a_W T_W + a_N T_N + a_S T_S \tag{6}$$

with, for instance, the east coefficient being given by

$$a_E = -\left(\frac{1}{2} - \alpha_e\right) C_e + \beta_e D_e, \tag{7}$$

where

$$C_e = (\rho U)_e \delta y \quad \text{and} \quad D_e = \left.\frac{K}{C_p}\frac{\delta y}{\Delta x}\right|_e \tag{8}$$

are the convective and diffusive fluxes, respectively. The remaining coefficients are similarly defined and they can be found in Ref. [11]. Moreover, with the help of Eq. (8), the control-volume Peclet number, Eq. (5), can be put in the form

$$Pe_e = \frac{C_e}{D_e} \tag{9}$$

which is in accordance to its physical meaning.

3.2. Multigrid method

Assembling Eq. (6) for each control volume inside the domain defines a linear algebraic equation system of the form

$$\mathbf{A}_k \mathbf{T}_k = \mathbf{b}_k, \tag{10}$$

where $\mathbf{A}_k$ is the *matrix of coefficients*, $\mathbf{T}_k$ is the *matrix of unknowns* and $\mathbf{b}_k$ is the matrix that accommodates possibly remaining terms. Subscript k refers to the grid level, with $k = 1$ corresponding to the coarsest gird and $k = M$ to the finest grid.

Multigrid is here implemented according to the CS formulation, in which one seeks coarse-grid approximations for the correction $\mathbf{t}_k$ of the quantity being numerically solved, which is defined as

$$\mathbf{t}_k = \mathbf{T}_k - \bar{\mathbf{T}}_k \tag{11}$$

with $\bar{\mathbf{T}}_k$ being an *intermediate value* resulting from a small number of smoothing iterations applied to Eq. (10). For a linear problem one shows [3,4,18] that $\mathbf{t}_k$ is the solution of

$$\mathbf{A}_k \mathbf{t}_k = \mathbf{r}_k, \tag{12}$$

where the *residue* is given by

$$\mathbf{r}_k = \mathbf{b}_k - \mathbf{A}_k \bar{\mathbf{T}}_k. \tag{13}$$

In the CS formulation, Eq. (12) is approximated by means of a coarse-grid equation

$$\mathbf{A}_{k-1} \mathbf{t}_{k-1} = \mathbf{r}_{k-1} \tag{14}$$

and the *restriction operator* I_k^{k-1} is used to obtain

$$\mathbf{r}_{k-1} = I_k^{k-1} \mathbf{r}_k. \tag{15}$$

A certain number of smoothing iterations is then performed on Eq. (14) at this lower grid level, resulting in an approximation for the correction $\bar{\mathbf{t}}_{k-1}$, which is in turn taken back to the fine grid by the *prolongation operator* I_{k-1}^k

$$\bar{\mathbf{t}}_k = I_{k-1}^k \bar{\mathbf{t}}_{k-1} \tag{16}$$

in order to update the intermediate value according to

$$\mathbf{T}_k^{\text{new}} = \bar{\mathbf{T}}_k + \bar{\mathbf{t}}_k. \tag{17}$$

The sequence as how all previous operations are concatenated through all existing k values (i.e., grid levels) is what distinguishes the so-called *V-cycle* from the *W-cycle* [4].

The residue restriction, Eq. (15), is accomplished by summing up the fine-grid residues corresponding to the four control volumes that compose the coarse-grid one. On the other hand, coefficients in matrix $\mathbf{A}_k$ contain diffusive and convective contributions, Eqs. (7) and (8), and they need special treatment when changing grid level. Diffusive terms are recalculated since they depend upon grid geometry while fine-grid mass fluxes (convective terms) are summed up at control-volume faces, for the sake of continuity. The rationale and further details of such procedures can be found in Refs. [1,5,7,8,10,12–14,17,20].

4. Results and discussion

Computer code was written in FORTRAN 90 language and numerical simulations were conducted in an IBM PC, with Pentium 166 MHz microprocessor. Grid independence is achieved from 18×18 meshes (including dimensionless control volumes, i.e., grid points located on the boundary) as seen in Fig. 3(a), for which $U = V = 0$ (pure conduction). Temperature profiles shown were calculated along the y-direction with $x = L_x/2$ and the curve named 'exact' corresponds to Eq. (2) evaluated at the identical midpoint.

For this same situation, Fig. 3(b) compares the exact solution, Eq. (2), to those numerically obtained employing 1-grid and 4-grids (V- and W-cycling strategies). One verifies that consistency holds for all numerical results, from which only a few points are plotted for clarity. In both 4-grid solutions, pre-

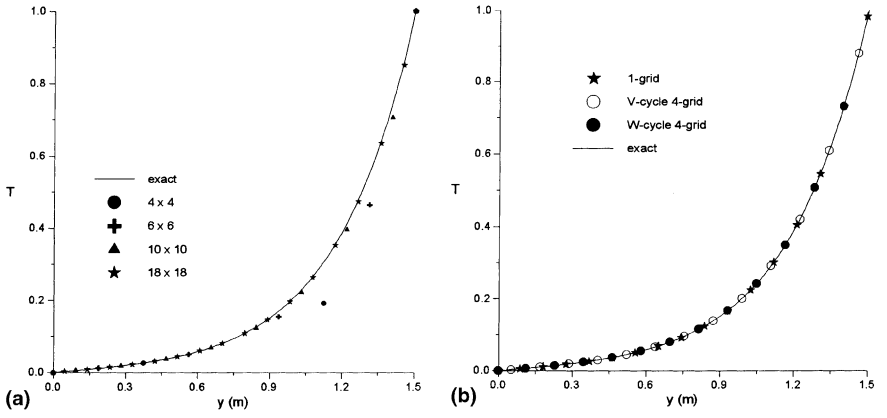

Fig. 3. (a) Grid influence on numerical solutions; (b) consistency of single-grid and multigrid solutions.

and post-smoothing iterations ($1 < k \leqslant M = 4$) are accomplished via *Gauss–Seidel* (GS) algorithm while coarsest-grid sweeps ($k = 1$) are via the *Trio-Diagonal Matrix Algorithm* – TDMA [9].

For a first study, numerical solutions of the strictly conductive problem ($U = V = 0$) are compared to those of a conductive–convective one ($U = -V = 10$ m/s) as far as the normalized residue reduction history is concerned. In the cases reported, the finest grid ($k = M$) always has $NI \times NJ$ finite volumes, being $NI = 130$ and $NJ = 194$ (including dimensionless boundary volumes) and a maximum of 6-grid levels is considered ($M \leqslant 6$). The cycling strategy assigns $\nu^{cg} = 5$ for the number of coarsest-grid iterations and $\nu^{pre} = \nu^{post} = 2$ for the number of pre- and post-smoothing iterations. Both V-cycle and W-cycle are examined. The residue is normalized and calculated *in the finest grid* according to

$$R = \sqrt{\sum_{ij}(r_{ij}^2)/(NI-2)(NJ-2)}, \quad r_{ij} = a_P T_P - \left(\sum_{nb} A_{nb} T_{nb}\right), \tag{18}$$

where subscript ij identifies a given control volume on the finest grid and nb refers to its neighboring control volumes. The Peclet numbers shown in figures are based on the uniform finest-grid spacing, Δx and Δy. Substitution of these values and of those adopted for the fluid properties, K/C_p and ρ, in Eq. (5) leads to

$$Pe\_x = 0.0078125\,U, \quad Pe\_y = 0.0078125\,V. \tag{19}$$

Figs. 4(a)–(d) plot the normalized residue level against the CPU time from 1-grid (1g) and V- and W-cycle multigrid solutions (3g_V, 4g_V, ..., 3g_W, 4g_W, etc.). One can readily notice that all multigrid solutions have better performance than that of the single-grid one. Such improvement increases as more accurate results are requested. This feature is what makes multigrid methods attractive, justifying their growing usage.

The influence of the Peclet numbers can be verified by comparison of Figs. 4(a) and (b) and of Figs. 4(c) and (d). One verifies a notable CPU time reduction (approximately three times less) for the same normalized residue level as Pe_x and Pe_y become non-zero. A possible reason can be related to the fact that boundary conditions are 'swept' faster into the domain for higher U, V (hence for higher Pe_x and Pe_y) in virtue of the convection mechanism.

Comparing Figs. 4(a) and (b) to Figs. 4(c) and (d), it is worth noting that the W-cycle solutions converge more quickly than the V-cycle ones for the same Pe_x and Pe_y. This is due to the fact that for the strategy adopted, $\nu^{cg} = 5$ and $\nu^{pre} = \nu^{post} = 2$, the larger relative time spent in coarse meshes in the W-cycle is such that it allows a more efficient smoothing of long wavelength error components. However, patterns of that kind can be altered, as it will be presented shortly.

Results also suggest the existence of an optimum number of grid levels, which varies with Pe_x, Pe_y and the type of multigrid cycle. Utilization of 5- or

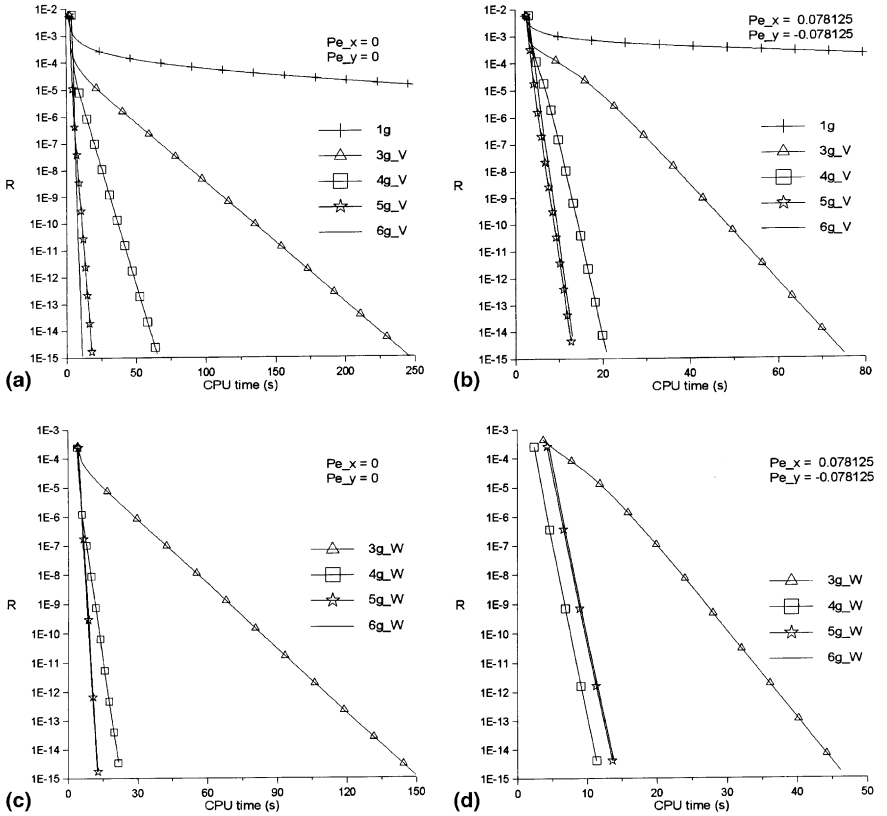

Fig. 4. Residue reduction histories: (a) $U = V = 0$, 1-grid and V-cycle multigrid solutions; (b) $U = -V = 10$ m/s, 1-grid and V-cycle multigrid solutions; (c) $U = V = 0$, W-cycle multigrid solutions; (d) $U = -V = 10$ m/s, W-cycle multigrid solutions.

6-grid levels is suitable for V-cycle solutions as well as for the null Peclet number W-cycle solution (Figs. 4(a)–(c)). On the other hand, the non-zero counterpart achieved better performance employing 4-grid (Fig. 4(d)), as the computational effort related to the value transfers among grids became relevant. It is important to note that such time expenditure in W-cycle is greater than in the V-cycle in a multigrid complete iteration.

As restriction and prolongation operations introduce imprecision to values being transferred, one should expect the computational effort to be sensitive to the number of smoothing sweeps in each grid level. In other words, once the numerical solution has reached an accuracy comparable to the errors introduced by the value transfer operators, it is of no use keep iterating in a that grid level.

The next two figures help to analyze such 'over-smoothing' waste of time. In Fig. 5(a) the number of pre- and post-smoothing iterations are fixed at

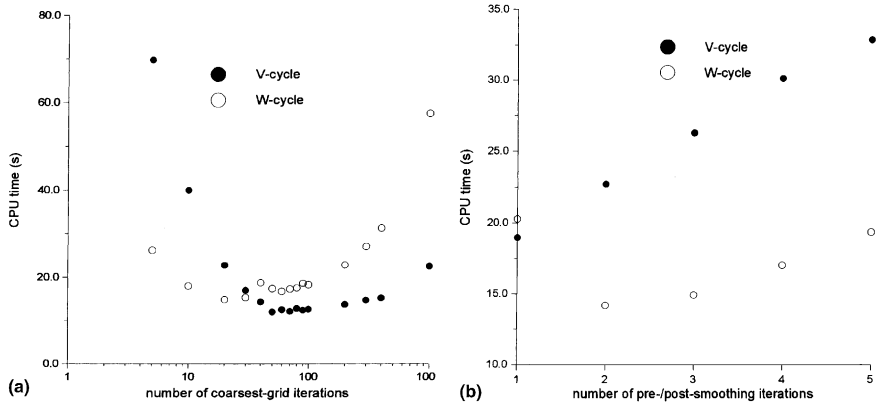

Fig. 5. Influence of the number of smoothing iterations, $U = V = 0$, $M = 4$, TDMA in all levels: (a) $\nu^{\mathrm{pre}} = \nu^{\mathrm{post}} = 2$ fixed and ν^{cg} varying; (b) $\nu^{\mathrm{cg}} = 20$ fixed and $\nu^{\mathrm{pre}} = \nu^{\mathrm{post}}$ varying.

$\nu^{\mathrm{pre}} = \nu^{\mathrm{post}} = 2$ while the number of coarsest-grid iterations ν^{cg} is free to vary. In Fig. 5(b) $\nu^{\mathrm{pre}} = \nu^{\mathrm{post}}$ are allowed to vary with $\nu^{\mathrm{cg}} = 20$ constant. For these new tests, the remaining algorithm parameters are fixed, namely, $U = V = 0$, $M = 4$ and TDMA applied in all grid levels $(1 \leqslant k \leqslant M)$.

From Fig. 5(a) one verifies that a small number of coarsest-grid iterations ν^{cg} may be less productive, i.e., long wavelength error components may not be sufficiently smoothed. Such effect is more pronounced on the V-cycle probably because it does not spend much time at such grid level within a complete multigrid iteration. On the other hand, the same argument might be used to explain the stronger influence of large ν^{cg} on the W-cycle (Fig. 5(a)) as well as the influence of large $\nu^{\mathrm{pre}} = \nu^{\mathrm{post}}$ on the V-cycle (Fig. 5(b).

Results presented in Figs. 5(a) and (b) also suggest the existence of an optimum number for either ν^{cg} or $\nu^{\mathrm{pre}} = \nu^{\mathrm{post}}$. However, these numbers cannot be easily determined a priori. This indetermination could be avoided by monitoring the ratio of residues after two successive iterations and using it as a criterion for deciding when to switch from one grid level to another. Hortmann et al. [5], point out that this practice is better indicated for single equation systems, which is the present case and it will be the subject of further investigations. With a coupled system of equations as for U, V, P (pressure) and T such practice is not easy to implement. In this case, one prefers to specify previously the number of sweeps, as done in the present work. However, many authors prefer to adopt this 'dynamic' criterion with distinct definitions of an 'global' residue ratio involving all quantities being numerically solved [6,10,17,19,20].

Finally, the influence of the choice of the iterative solution algorithm, namely, TDMA and GS, for each grid level is presented in Fig. 6 for both

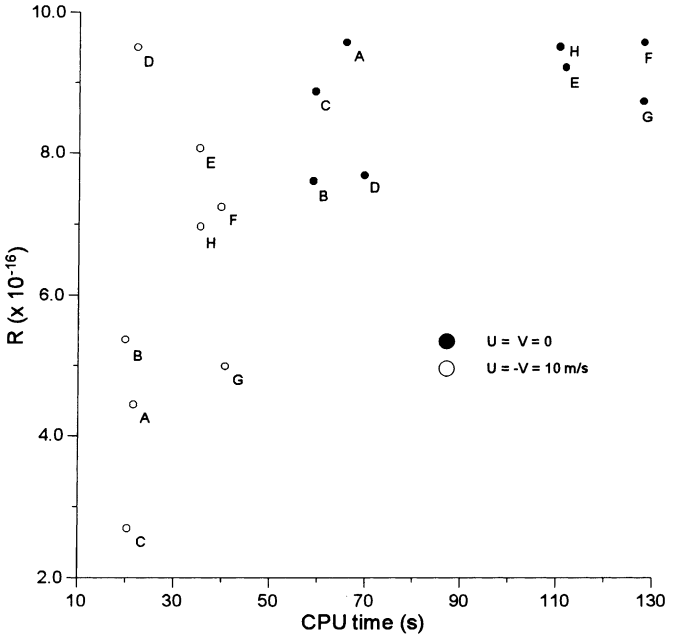

Fig. 6. Influence of the choice of iterative solution algorithms for $U = V = 0$ and $U = -V = 10$ m/s, $M = 4$, V-cycle. Key (number in parenthesis refers to the grid level): A – GS (4, 3, 2), TDMA (1); B – GS (4, 3), TDMA (2, 1); C – GS (4), TDMA (3, 2, 1); D – TDMA (4, 3, 2, 1); E – TDMA (4, 3, 2), GS (1); F – TDMA (4, 3), GS (2, 1); G – TDMA (4), GS (3, 2, 1); H – GS (4, 3, 2, 1).

$U = V = 0$ and $U = -V = 10$ m/s. The remaining parameters are set as V-cycle and $M = 4$. Points are identified by capital letters and they correspond to a given combination of TDMA and GS. The number in parenthesis (in the key) indicates the grid level in which the solution algorithm is applied.

It is interesting to note that certain combinations, particularly A, B and C, achieve better performance than others, like E, F and H. It is worth remembering [9] that the GS algorithm visits the control volumes of the domain *one by one in a one-way sweep* whereas the TDMA performs a *two-way sweep of an entire row* (or column) of control volumes. Therefore, one should expect the computational effort to be sensitive to the choice of the solution algorithm for different mesh sizes.

5. Concluding remarks

The multigrid method was implemented according to the CS conception to numerically solve a two-dimensional steady-state conductive–convective

problem over a rectangular domain. The velocity field inside the domain and the temperature at its four boundaries were taken as fixed conditions. Structured, orthogonal and regular meshes were used to discretize the energy equation through a finite volume formulation and the WUDS was employed as interpolation function.

Parameters were varied and critical values were sought in order to optimize the overall algorithm performance, including the control-volume Peclet numbers (*Pe_x* and *Pe_y*), number of grid levels, multigrid cycling, number of smoothing sweeps and choice of iterative solution algorithm. Important to mention is the fact that in general these values cannot be easily determined a priori.

Results suggested a reduction in the computational effort required for increasing values of the velocity components (and hence of *Pe_x* and *Pe_y*). They also pointed out the existence of an optimum number of grid levels (not below 4), which depended on the Peclet numbers and on the type of multigrid cycle employed.

As far as the cycling strategy is concerned, results indicated the existence of optimum numbers of coarsest-grid sweeps, namely, $\nu^{cg} \sim 20$ for V-cycle and $\nu^{cg} \sim 60$ for W-cycle, and of pre- and post-smoothing iterations, $\nu^{pre} = \nu^{post} = 1$ for V-cycle and $\nu^{pre} = \nu^{post} = 2$ for W-cycle. Finally, the computational effort showed to be dependent on the choice of the solution algorithm according to the grid level and hence to the grid size.

Acknowledgements

Authors would like to thank CNPq (Brazil) for their financial support throughout this research, undertaken at the *Computational Transport Phenomena Laboratory* of the Department of Energy, LCFT-ITA, Brazil.

References

[1] L. Bai, N.K. Mitra, M.C. Fiebig, A. Kost, A multigrid method for predicting periodically fully developed flow, Int. J. Numer. Methods Fluids 18 (1994) 843–852.
[2] R.B. Bird, W.E. Stewart, E.N. Lightfoot, Transport Phenomena, Wiley, New York, 1960.
[3] A. Brandt, Multi-level adaptive solutions to boundary-value problems, Math. Comp. 31 (138) (1977) 333–390.
[4] W. Hackbusch, Multigrid Methods and Applications, Springer, Berlin, 1985.
[5] M. Hortmann, M. Peric, G. Scheuerer, Finite volume multigrid prediction of laminar convection: bench-mark solutions, Int. J. Numer. Methods Fluids 11 (1990) 189–207.
[6] B.R. Hutchinson, P.F. Galpin, G.D. Raithby, Application of additive correction multigrid to the coupled fluid flow equations, Numer. Heat Transfer 13 (1988) 133–147.
[7] Y. Jiang, C.P. Chen, P.K. Tucker, Multigrid solutions of unsteady Navier–Stokes equations using a pressure method, Numer. Heat Transfer A 20 (1991) 81–93.

[8] D.S. Joshi, S.P. Vanka, Multigrid calculation procedure for internal flows in complex geometries, Numer. Heat Transfer B 20 (1991) 61–80.
[9] S.V. Patankar, Numerical Heat Transfer and Fluid Flow, McGraw-Hill, New York, 1980.
[10] M. Peric, M. Rüger, G. Scheuerer, A finite volume multigrid method for calculating turbulent flows, in: The Seventh Symposium on Turbulent Shear Flows, Stanford University, 1989, pp. 7.3.1–7.3.6.
[11] J.A. Rabi, Application of the multigrid method to the numerical solution of two-dimensional flow and heat transfer, M.S. thesis, Instituto Technológico de Aeronáutica, São José dos Campos, Brazil, 1988 (in Portuguese).
[12] J.A. Rabi, M.J.S. de Lemos, Influence of Peclet number on numerical solution of two-dimensional convection–diffusion problems using the multigrid method, in: Proc. COBEM97 – 14th Braz. Congr. Mech. Eng. (on CD-ROM), Bauru, São Paulo, Brazil, 1997 (in Portugese).
[13] J.A. Rabi, M.J.S. de Lemos, Multigrid numerical solution of incompressible laminar recirculating flows, in: Proc. ENCIT-98 – 7th Braz. Cong. Eng. Th. Sci., Rio de Janeiro, RJ, Brazil, vol. 2, 1998, pp. 915–920.
[14] J.A. Rabi, M.J.S. de Lemos, The effects of Peclet number and cycling strategy on multigrid numerical solutions of convective–conductive problems, in: Proc. 7th AIAA/ASME Joint Thermophysics & Heat Transfer Conference, Paper AIAA-98-2584, Albuquerque, NM, 1998.
[15] G.D. Raithby, Prediction of dispersion by surface discharge, Basin Investigation and Modeling Section, Canada Centre for Inland Waters, Canada, 1976.
[16] G.D. Raithby, K.E. Torrance, Upstream-weighted differencing schemes and their application to elliptic problems involving fluid flow, Comput. & Fluids 2 (1974) 191–206.
[17] P.S. Sathyamurthy, S.V. Patankar, Block-correction-based multigrid method for fluid flow problems, Numer. Heat Transfer B 25 (1994) 375–394.
[18] K. Stüben, U. Trottenberg, Multigrid Methods, Lecture Notes in Math., No. 960, Springer-Verlag, Berlin, 1982, pp. 1–176.
[19] M.C. Thompson, J.H. Ferziger, An adaptive multigrid technique for the incompressible Navier–Stokes equations, J. Comput. Phys. 82 (1989) 94–121.
[20] S.P. Vanka, Block-implicit multigrid calculation of two-dimensional recirculating flows, Comput. Methods Appl. Mech. Eng. 86 (1986) 29–48.